)URNAL OF MOLECULAR SPECTROSCOPY **146,** 493–512 (1991)

A Microwave Spectral and ab initio Investigation of O_3–H_2O

J. Z. GILLIES

Department of Chemistry, Siena College, Loudonville, New York 12221

C. W. GILLIES

Department of Chemistry, Rensselaer Polytechnic Institute, Troy, New York 12180

R. D. SUENRAM AND F. J. LOVAS

Molecular Physics Division, National Institute of Standards and Technology, Gaithersburg, Maryland 20899

T. SCHMIDT

Institut fur Organishe Chemie, Universitat Köln, Köln, Federal Republic of Germany

AND

D. CREMER

Theoretical Chemistry, University of Göteborg, Kemigarden 3, S-41296 Göteborg, Sweden

Microwave spectra of O_3–H_2O, O_3–$H_2{}^{18}O$, O_3–HDO, and O_3–D_2O have been observed with a pulsed-beam Fabry–Perot cavity Fourier-transform microwave spectrometer. Two tunneling states, designated A_1 and A_2, are found for the normal and dideuterated isotopic forms, while only one state is observed for the O_3–HDO isotope. The A_1 spectra of O_3–H_2O, O_3–$H_2{}^{18}O$, and O_3–D_2O as well as the O_3–HDO spectrum were fit to a Watson asymmetric top Hamiltonian, giving A = 11 960.584(5), B = 4174.036(8), and C = 3265.173(8) in MHz for O_3–H_2O. The A_2 states of O_3–H_2O and O_3–D_2O could not be fit to a Watson Hamiltonian. This result, when combined with the large frequency splittings and the observed nuclear spin statistics for the O_3–H_2O and O_3–D_2O isotopic forms, suggests that there is a low barrier to internal rotation of water. The tunneling motion may also involve ozone through a concerted internal rotation of both monomer subunits. Stark effect measurements of a- and c-type transitions for O_3–H_2O give the electric dipole components μ_a = 1.014(2) D and μ_c = 0.522(6) D. The dipole and moment of inertia data indicate that the complex has C_s symmetry with water and the unique oxygen of ozone lying in the symmetry plane. This plane bisects the OOO angle of ozone. The distance between the centers of mass of ozone and water is 2.957(2) Å. From the microwave data and ab initio calculations at the MP2/6-31G(d, p) and MP4(SDTQ)/6-31G(d, p) level of theory it is found that the terminal oxygens of ozone are tilted toward one of the nonequivalent hydrogen atoms in water. Furthermore, the calculations reveal that O_3 and H_2O adopt an orientation within the complex that guarantees maximal stabilization by electric dipole–dipole attraction.

0022-2852/91 $3.00

I. INTRODUCTION

Ozone is a reactive species, and its chemistry has been investigated extensively in the gas phase and in solution. The chemistry of ozone is important in the upper atmosphere due to the depletion of the ozone layer by a series of reactions involving halogenated hydrocarbons. Ozone is also involved in atmospheric pollution which includes both smog formation and acid rain through sulfur dioxide oxidation.

Muenter and co-workers have pointed out that the weak, long-range van der Waals interactions between chemical species are relevant to atmospheric studies (*1*). Both molecular-beam-electric-resonance and pulsed-nozzle Fourier-transform microwave spectroscopies provide accurate structural and dynamical properties of van der Waals complexes (*2, 3*). These methods have been used to characterize a large number of weakly bound complexes (*4*). However, argon–ozone and ethylene–ozone are the only van der Waals complexes reported which contain ozone (*5, 6*).

Since ozone is such a chemically reactive species, studies of ozone bound to other simple molecules are useful in characterizing the weak, long-range interactions. The ozone–water complex is particularly important because both gas phase and solution chemistry involving ozone and water have arisen in a number of atmospheric problems (*7*). This paper reports the study of the ozone–water van der Waals complex, O_3–H_2O, using a pulsed-nozzle Fourier-transform microwave spectrometer. Structural results are obtained from the analysis of rotational spectra of four isotopic species, together with the electric dipole moment derived from Stark effect measurements. The spectral data also provide insight into the internal dynamics of the complex. In addition to the microwave investigation, an extensive ab initio study has been carried out in order to substantiate the experimental results and to elucidate forces that determine the structure and stability of the complex. A description of the geometry and electronic nature of the O_3–H_2O complex has been obtained by combining the experimental and theoretical results.

II. EXPERIMENTAL DETAILS

The rotational spectra of the O_3–H_2O complex and its isotopes were obtained using a Fabry–Perot-cavity Fourier-transform microwave spectrometer (*8*) with a modified pulsed-nozzle jet source (*9, 10*). The strongest transitions of O_3–H_2O were observed with good signal-to-noise ratios ($S/N \sim 10$) from a single microwave pulse. Line frequencies have estimated measurement uncertainties of 4 kHz, and the linewidths are $\sim 10^{-6}$ of the microwave pump frequency.

Ozone was prepared by passing oxygen through a Welsbach ozonator into a glass trap containing silica gel maintained near dry ice temperature. In the initial work on O_3–H_2O, water was expanded into the evacuated inlet line. The line was then pressurized to 3–6 psi by flowing argon through the silica gel trap containing ozone and into the inlet line. A pulsed solenoid valve with a 0.5-mm orifice delivered this gas mixture into the Fabry–Perot cavity. Rotational transitions of water dimer (*11*), argon–ozone (*6*), and ozone (*12*) were monitored to be certain both monomers were present during the spectral searches for O_3–H_2O transitions. Much of the spectral work including the deuterium isotopes utilized a reservoir pulsed valve (*9, 10*). Water was placed in the reservoir which is in the immediate vicinity of the nozzle orifice. The

TABLE I

A_1 State Rotational Transitions of Ozone–Water Isotopic Species

$J'K_{-1},K_{+1}$ - $J''K_{-1},K_{+1}$	O_3-H_2O		O_3-$H_2{}^{18}O$		O_3-D_2O	
	ν_{obsd}[a] (MHz)	$\Delta\nu$[b] (kHz)	ν_{obsd}[a] (MHz)	$\Delta\nu$[b] (kHz)	ν_{obsd}[a] (MHz)	$\Delta\nu$[b] (kHz)
1_{01} - 0_{00}	7439.082	1				
1_{11} - 1_{01}	7786.320	-1	8061.067	0		
3_{03} - 2_{11}	12342.944	-5	11010.079	1	10807.519	-3
2_{12} - 1_{11}	13968.332	5	13169.113	-1	12950.396	0
2_{02} - 1_{01}	14802.659	0	13915.556	0	13665.761	3
2_{11} - 1_{10}	15783.990	-1	14773.495	0	14484.394	-3
1_{10} - 0_{00}	16133.402	-1	15849.946	-1	15600.424	-3
3_{13} - 2_{12}	20906.313	9	19718.152	0	19392.602	11
3_{03} - 2_{02}	22018.597	-6	20731.416	-2	20367.048	-10
3_{22} - 2_{21}	22306.768	-2			20569.937	-2
3_{21} - 2_{20}	22602.321	-2			20778.811	-2
2_{21} - 2_{11}	23354.933	0				
3_{12} - 2_{11}	23625.113	8	22121.493	0	21690.671	7
2_{11} - 1_{01}	24478.309	-4	23636.898	2	23225.294	0
4_{14} - 3_{13}					25798.278	-1

[a]The estimated uncertainty in the frequency measurements is 4 kHz for the normal and oxygen-18 isotopic species and 10 kHz for the dideuterated isotopic species due to unresolved deuterium hyperfine structure.

[b]$\Delta\nu$ is the observed minus calculated frequency in kHz from the least squares fit.

reservoir nozzle was located directly above the diffusion pump which warmed the reservoir to 35–40°C. The O_3–$H_2{}^{18}O$ spectrum was assigned using oxygen-18 enriched water (99%). Enriched D_2O (99%) was used to produce O_3–D_2O. The O_3–HDO isotope was assigned concurrently with O_3–D_2O. Rapid exchange of H_2O (which originated from the silica gel trap and the inlet line walls) with D_2O produced sufficient concentrations of O_3–HDO for the spectral assignments. Rotational transitions of deuterated water dimer (*10, 13*) were used to determine the deuterium exchange in water, and the spectrum of $(HDO)_2$[1] was monitored to verify the presence of HDO.

III. SPECTRAL MEASUREMENTS AND ASSIGNMENTS

The observed microwave rotational transitions of O_3–H_2O, O_3–$H_2{}^{18}O$, O_3–D_2O, and O_3–HDO are listed in Tables I–III. Both *a*- and *c*-type transitions were observed for the A_1 state of O_3–H_2O, O_3–$H_2{}^{18}O$, and O_3–D_2O as well as the O_3–HDO isotopic species, while only several *a*-type transitions have been observed for a second state, labeled the A_2 state, of O_3–H_2O and O_3–D_2O. The relative intensities of the A_1 and A_2 transitions of O_3–H_2O were approximately 1:3, respectively, while for O_3–D_2O the

[1] The $J = 1 \leftarrow 0$ *B* and *A* state lines of $(HDO)_2$ were measured at 10 477.401 and 13 120.121 MHz, respectively. The $J = 2 \leftarrow 1$ *B* and *A* states have transition frequencies of 22 277.273 and 21 915.533 MHz, respectively.

TABLE II

A_2 State Transitions and A_1 Minus A_2 Transition Splittings ($\Delta\nu$) for O_3–H_2O and O_3–D_2O

$J'K_{-1},K_{+1}$-$J''K_{-1},K_{+1}$	O_3-H_2O		O_3-D_2O	
	$\nu_{obsd.}$[a] (MHz)	$\Delta\nu$[b] (MHz)	$\nu_{obsd.}$[a] (MHz)	$\Delta\nu$[b] (MHz)
2_{12} - 1_{11}	13449.028	519.304	12424.866	525.530
2_{02} - 1_{01}	14329.083	473.576	13217.229	448.532
2_{11} - 1_{10}	15594.563	189.427	14333.029	151.365

[a]The estimated uncertainty in the frequency measurements is 4 kHz.

[b]$\Delta\nu$ is the observed A_1-A_2 transition splittings.

corresponding relative intensities were about 2:1. No attempt was made to locate the A_2 state spectrum of O_3–$H_2{}^{18}O$. The A_1 state transitions of O_3–H_2O, O_3–$H_2{}^{18}O$, and O_3–D_2O and the lines from the O_3–HDO species were fit to the Watson (*14*) asym-

TABLE III

Rotational Transitions of O_3–HDO Isotopic Species

$J'K_{-1},K_{+1}$-$J''K_{-1},K_{+1}$	F'-F''	$\nu_{obsd.}$[a] (MHz)	$\Delta\nu$[b] (kHz)
1_{11} - 1_{01}		7816.100[c]	1
	1-0	7816.064	1
	2-2	7816.098	0
	2-1	7816.119	3
3_{03} - 2_{11}		11681.159[c]	2
	3-2	11681.135	1
2_{12} - 1_{11}		13487.325[c]	-2
	3-2	13487.329	-1
2_{02} - 1_{01}		14262.488[c]	-1
	3-2	14262.490	0
2_{11} - 1_{10}		15162.482[c]	1
	1-1	15162.452	-1
	3-2	15162.485	1
	1-0	15162.520	1
1_{10} - 0_{00}		15817.336[c]	1
	0-1	15817.296	4
	2-1	15817.331	-1
	1-1	15817.358	0
4_{04} - 3_{12}		17011.598[c]	-1
	4-3	17011.571	-3
	5-4	17011.608	2
3_{13} - 2_{12}		20191.235[d]	11
3_{03} - 2_{02}		21234.993[d]	-5
3_{12} - 2_{11}		22700.068[d]	2

[a]The measurement uncertainty is estimated to be 4 kHz.

[b]$\Delta\nu$ is observed minus calculated frequency in kHz from the least squares fit to the coupling constants and the unsplit frequency.

[c]Hypothetical unsplit center frequencies are obtained from the hyperfine fit.

[d]No hyperfine components are resolved; transition used only for the unsplit line fit.

TABLE IV

Spectral Constants of Ozone–Water Isotopic Species[a]

Spectral Constant	O_3-H_2O	O_3-H_2O^{18}	O_3-HDO	O_3-D_2O
Rotational Constants				
A (MHz)	11960.584 (5)[b]	11956.150 (1)	11817.451 (3)	11787.689 (8)
B (MHz)	4174.036 (8)	3894.922 (7)	4001.115 (2)	3813.725 (12)
C (MHz)	3265.173 (8)	3091.740 (8)	3162.508 (1)	3045.916 (11)
Δ_J (MHz)	0.0321 (1)	0.02903 (3)	0.0341 (1)	0.0277 (2)
Δ_{JK} (MHz)	0.3077 (6)	0.2727 (2)	0.3128 (6)	0.2497 (8)
Δ_K (MHz)	0.042 (2)	0.04[c]	0.04[c]	0.04[c]
δ_J (MHz)	0.00706 (9)	0.00598 (2)	0.00718 (5)	0.0056 (1)
δ_K (MHz)	0.201 (3)	0.2[c]	0.2[c]	0.157 (5)
P_{bb}[d] (μÅ^2)	37.9775	37.9883	38.1290	38.1389
Deuterium Hyperfine Constants				
eQq_{aa} (kHz)			-59.7 (4)	
eQq_{bb} (kHz)			-27.7 (4)	
eQq_{cc} (kHz)			87.4 (2)	
Dipole Moment				
μ_{total} (Debyes)	1.140 (2)		1.128 (6)	1.145 (1)
μ_a (Debyes)	1.014 (2)		0.958 (5)	0.935 (1)
μ_c (Debyes)	0.522 (2)		0.596 (7)	0.661 (2)

[a]The spectral constants for O_3-$H_2{}^{16}O$, O_3-$H_2{}^{18}O$, and O_3-D_2O are obtained from fits of A_1 state lines.
[b]Uncertainties in parentheses are one standard deviation of the least squares fit.
[c]Fixed at this value in the fit.
[d]$P_{bb} = 1/2(I_a+I_c-I_b)$.

metric top Hamiltonian in the I^r representation with the resulting spectral constants given in Table IV. Attempts to fit the A_2 state transitions with this model were unsuccessful. For the initial assignments, Stark effect measurements were employed to identify the rotational quantum numbers. The assignments of the A_2 state transitions in Table II were based on Stark effect measurements which closely resembled the Stark effect of the corresponding A_1 transitions as shown in Fig. 1 for O_3–H_2O. A nearly identical plot was obtained for the $J = 2$–1 transitions of O_3–D_2O. In addition, exhaustive searches with D_2O in the a-type $J = 2$–1 region of O_3–D_2O and O_3–HDO have shown that no other lines are present. This supports the A_2 assignment of O_3–D_2O in Table II, and it also provides strong evidence for the absence of a second state for O_3–HDO. A number of transitions have been found in the a-type $J = 3$–2 regions of O_3–H_2O and O_3–D_2O. Additional work including microwave double resonance experiments are planned to obtain firm assignments of these lines.

Deuterium nuclear electric quadrupole hyperfine structure was resolved for the O_3–HDO species (see Fig. 2) and is summarized in Table III. The results of the hyperfine structure analysis are given in Table IV. For the O_3–D_2O species the deuterium hy-

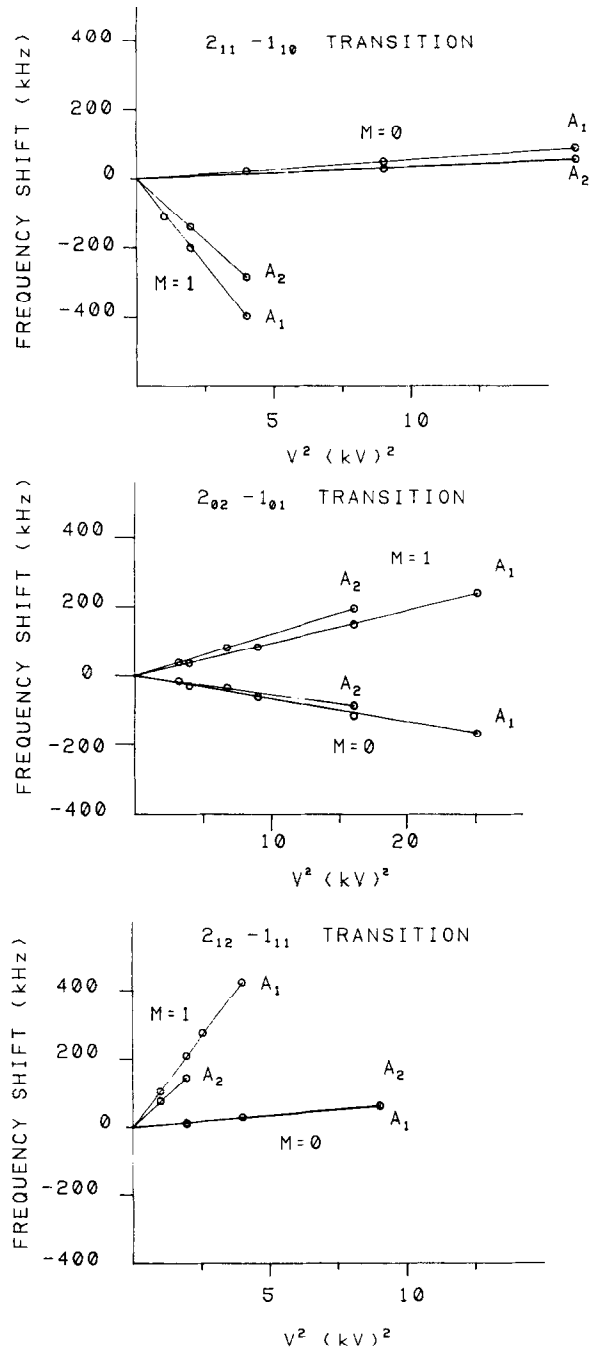

FIG. 1. Plots of $\Delta\nu$ versus V^2 for μ_a-type $J = 2$–1 for A_1 and A_2 Stark transitions of O_3–H_2O.

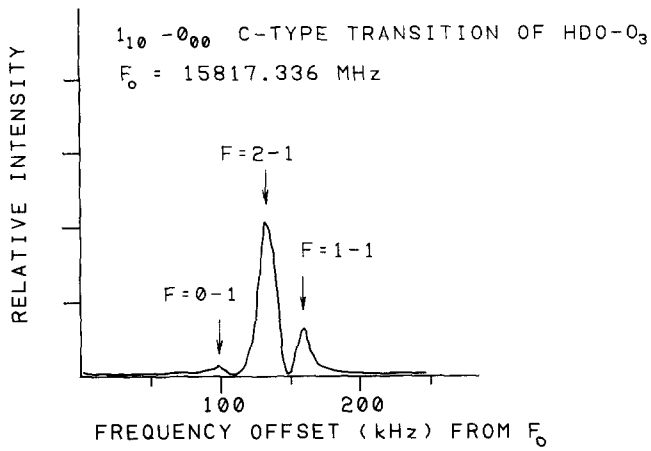

FIG. 2. The 1_{10}–0_{00} c-type transition of HDO–O_3 illustrating the deuterium hyperfine components.

perfine structure was at best partially resolved which prevented the determination of the hyperfine constants for this species.

IV. ELECTRIC DIPOLE MOMENTS

The electric dipole moments of O_3–H_2O, O_3–HDO, and O_3–D_2O were determined by measuring the Stark effects of a number of different rotational transitions. Stark effect measurements in a Fabry–Perot-cavity pulsed-beam spectrometer were described previously (*10, 15*). The effective electric field between the plates was calibrated using the known dipole moment of OCS (*16*).

$|M_J| = 0, 1$ components of the 2_{12}–1_{11}, 2_{02}–1_{01}, and 2_{11}–1_{10} transitions and the $M_J = 0$ component of the 1_{10}–0_{00} transitions were included in 36 Stark shift measurements of the A_1 state of O_3–$H_2{}^{16}O$. Parallel arrangement of the microwave electric field with the applied dc field gave $\Delta M_J = 0$ selection rules for all transitions. In addition, for the 1_{10}–0_{00} transition $|\Delta M_J| = 1$ selection rules were observed by rotating the microwave electric field 90° so that it was perpendicular to the applied field. All the data were least-squares fit to the three dipole components along the principal axes using second-order perturbation theory (*17*). The value of μ_b was found to be 0.06 ± 0.15 D; consequently, the data were refit with $\mu_b = 0$ to the two remaining nonzero dipole components which yielded $\mu_a = 1.014(2)$ D and $\mu_c = 0.522(6)$ D, and the standard deviation of the fit was 3 kHz in both cases which is close to the measurement uncertainty of 4 kHz. Similar measurements on O_3–HDO and the A_1 state of O_3–D_2O were performed employing the same methods discussed above. The results of least-squares fits of these data gave the dipole moment components listed in Table IV.

V. STRUCTURE

Moment of inertia analysis. In the course of determining the structure of O_3–H_2O several inconsistencies arose. In order to describe these problems, we will first outline the aspects of the structure which can be firmly established from the experimental

results. Since μ_b was found to be zero in the dipole moment analysis, the C_2 axes of water and ozone must lie in the a, c-symmetry plane of the complex. The large out-of-plane second moment of the complex, $P_{bb} = 1/2\,(I_a + I_c - I_b) = \sum m_i b_i^2$, does not change much upon ^{18}O substitution and very little with deuterium substitution in water (see Table IV). Hence, the isotopic change in P_{bb}, $\Delta P_{bb} = P_{bb}(O_3\text{–}H_2O) - P_{bb}$ (substituted species), for $O_3\text{–}H_2{}^{18}O$, $O_3\text{–}HDO$, and $O_3\text{–}D_2O$, is -0.01076, -0.1516, and -0.1614 u Å^2, respectively, which indicates that the oxygen and two hydrogen atoms of water are located essentially in the a, c plane (*18*). In free ozone the a principal axis is perpendicular to the C_2 axis and lies in the molecular plane. The out-of-plane second moment of $O_3\text{–}H_2O$ ($P_{bb} = 37.9775$ u Å^2) is only 0.068 u Å^2 larger than the a second moment of free ozone ($P_{aa} = 37.9095$ u A^2) (*19*). If the water unit and central oxygen of ozone are located in the a, c plane of the complex, P_{bb} of the complex should be approximately equal to P_{aa} of free ozone when the planes of the two monomer units are perpendicular, i.e., the terminal oxygens of ozone are located symmetrically out of the a, c plane. The P_{bb} values also provide further support for locating the hydrogens in the a, c plane since P_{bb} (complex) would have a contribution of $2m_H b_H^2 = 1.16$ u Å^2 from the hydrogens (and for deuterium $2m_D b_D^2 = 2.32$ u Å^2) if they were symmetrically placed out of the a, c plane. Thus, the orientation of the monomer planes is established as illustrated in Fig. 3. Comparing the total dipole moment of the complex, $\mu_T = 1.140$ D, with the vector addition of the μ_b dipole moment of each monomer suggests quite strongly that the monomer moments must be opposed. With $\mu_b(O_3) = 0.5324$ D (*19*) and $\mu_b(H_2O) = 1.8550$ D (*20*) even a complete cancellation of the moments would give a total dipole moment of 1.32 D

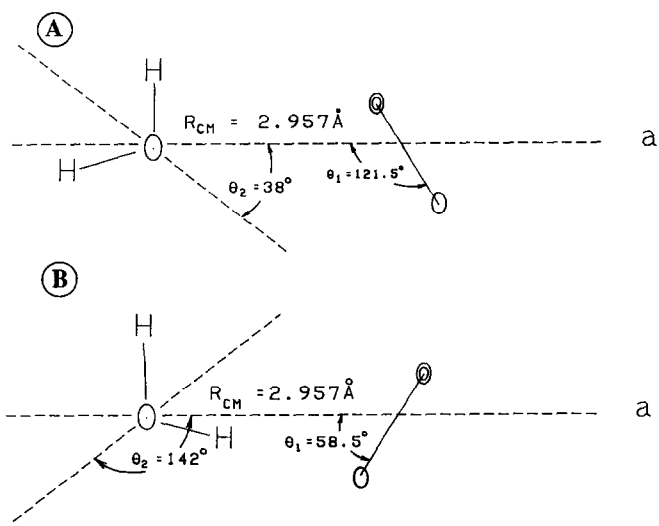

FIG. 3. Structures **A** and **B** of $O_3\text{–}H_2O$ obtained from the microwave analysis described in the text. The geometrical parameters of ozone–water are R_{cm}, the distance of the center of mass of ozone to the center of mass of water, θ_1, the angle between the C_2 axis of ozone and R_{cm}, and θ_2, the angle between R_{cm} and the C_2 axis of water. The two forms are distinguished from one another by the supplementary angles for θ_1 and θ_2.

for the complex (neglecting induced moment effects). This comparison provides a strong bias for orienting the C_2 axes of the monomers approximately parallel but with opposed monomer dipole moments as shown in Fig. 3.

For the structural fitting of isotopic moment of inertia data described below, the geometries of water and ozone are assumed to remain unchanged upon complex formation, which has been validated in a number of prior studies of dimeric complexes. With this assumption and the structural properties discussed above, there are then three parameters required to determine the O_3–H_2O structure. These are R_{cm}, the separation of the H_2O and O_3 centers of mass, θ_1, the angle between R_{cm} and the C_2 axis of O_3, and θ_2, the angle between R_{cm} and the C_2 axis of H_2O as defined in Fig. 3. The angle θ_2 is defined in a positive sense for clockwise rotation from R_{cm} to the C_2 axis of H_2O while for θ_1 anticlockwise rotation applies. Although it would be desirable to use the moments of each isotopic species separately to determine these parameters, this is possible only for R_{cm} which can be expressed as

$$I_b(O_3\text{–}H_2O) = I_c(H_2O) + I_a(O_3) + \mu(H_2O + O_3)R_{cm}^2, \qquad (1)$$

where $\mu(H_2O + O_3)$ is the reduced mass of the two monomer subunits. By using the reported values of $I_c(H_2O)$ (*20*) and $I_a(O_3)$ (*19*), R_{cm} is calculated to be 2.957 Å for O_3–H_2O, 2.955 Å for O_3–HDO, 2.953 Å for O_3–$H_2{}^{18}O$, and 2.966 Å for O_3–D_2O. The small decrease in R_{cm} for the first three isotopic species correlates with the expected decrease in the amplitude of the van der Waals stretching vibration with increased mass, while the 0.01 Å increase in R_{cm} for the D_2O species seems anomalous and suggests that its vibrationally averaged structure may differ from the other isotopic species.

Since the angular parameters θ_1 and θ_2 have no dependence upon the second moment $P_{bb} = \sum m_i b_i^2$, *only* $P_{aa} = \sum m_i a_i^2$ and $P_{cc} = \sum m_i c_i^2$ are useful inertial constants. Hence, the structural analysis requires the combination of the moments of inertia from at least two isotopic species to determine the three parameters. Least-squares fits of the second moments of inertia to R_{cm}, θ_1, and θ_2 were carried out for the isotopic combinations: (O_3–H_2O, O_3–$H_2{}^{18}O$), (O_3–H_2O, O_3–$H_2{}^{18}O$, O_3–HDO), and (O_3–H_2O, O_3–$H_2{}^{18}O$, O_3–D_2O). These fits employed the r_0 monomer geometries listed in Table V (*20*).[2] The results of these fits are listed in Table VI and yielded values of R_{cm} from 2.951 to 2.958 Å for structure **A** (upper structure of Fig. 3) which is reasonable when compared to the values obtained from Eq. (1). For the combination of isotopes which included the HDO species, the fits were found to converge for two supplementary angles of θ_1 with corresponding values of θ_2. The structures **A** and **B** which correspond to those fits have approximate antiparallel orientation of the dipole moments of the monomers, although the fit of structure **B** (acute value of θ_1) had the larger standard deviation. The θ_1 values for the structure **A** orientation (obtuse value of θ_1) ranged from 118° to 125°, i.e., a 7° range, while the θ_2 values show a 46° range depending on the choice of isotopic combinations. The second structure, **B**, obtained in the fit including the O_3–HDO species ($\theta_1 = 56°$, $\theta_2 = 135°$) is unreasonable due to the extremely short H . . . O atom distance of 1.81 Å and the fact that the hydrogen atom

[2] R(O–O) and θ(OOO) were obtained from an r_0 fit of the normal isotopic species of ozone (see Ref. (*19*) for the molecular constants).

TABLE V

Principal Moments of Inertia and Structural Parameters of Free Water and Ozone

Monomer	I_a (u·Å^2)	I_b (u·Å^2)	I_c (u·Å^2)
H_2O[a]	0.604641	1.16154	1.81609
O_3[b]	4.74373	37.8587	42.7038
Monomer Geometry	**R(X-O)**	**θ(XOX)**	
H_2O[a]	0.9565Å	104.9°	
O_3[c]	1.276Å	116.97°	

[a]Reference 20.

[b]Reference 19.

[c]Obtained from an r_0 fit of the moments of inertia of $^{16}O_3$ (reference 19).

is directed at the positive charge region of the central oxygen atom of ozone. Thus, the average values of $R_{cm} = 2.957(2)$ Å and $\theta_1 = 121.4 \pm 5°$ are well determined, but the angular orientation of the water unit via θ_2 is poorly determined due to the obvious inconsistency in the inertial moments for the HDO species and D_2O species. We carried out Kratichman substitution calculations as well, but these proved to be no more enlightening regarding the positions of the hydrogen atoms. Also listed in Table VI are the μ_a and μ_c dipole moment components derived from the vector sums of the monomer dipole moments for each fit. Due to the wide variation in θ_2, these show a wide range in values, and the best agreement with the experimental values is obtained for the fits employing the O_3–HDO species with $\theta_2 = 32.6°$.

TABLE VI

Structural Fits for O_3–H_2O for Various Combinations of Isotopic Species

Species:	O_3-H_2O, O_3-$H_2{}^{18}O$	O_3-$H_2{}^{16}O$, -$H_2{}^{18}O$, -HDO		O_3-$H_2{}^{16}O$, -$H_2{}^{18}O$, -D_2O
Form[a]:	A	A	B	A
R_{cm} (Å)	2.958(1)	2.957(2)	2.951(4)	2.956(1)
θ_1	120.7(2)°	125.0(14)°	56.0(28)°	118.4(7)°
θ_2	54.2(12)°	32.6(31)°	134.7(58)°	78.7(14)°
σ (uÅ^2)	0.006	0.18	0.35	0.08
Derived properties:				
$r_{O\text{-}O}$ (Å)	3.208(1)	3.174(7)	2.767(20)	3.172(5)
$r_{H\text{-}O}$ (Å)	2.836(18)	3.145(45)	1.811(21)	2.505(17)
<DO-a axis	74°	84°	83°	50°
μ_a (D)	0.830	1.268	1.023	0.134
μ_c (D)	1.034	0.541	0.859	1.349

[a]Form A is shown in the upper part of Fig. 3 and form B in the lower part.

Electric dipole moments. Another approach to determining angular orientation of the water unit is to employ the measured electric dipole moments and the deuterium quadrupole coupling constants of the complex and the monomer units to determine θ_2. For the dipole moments the projection formula for μ_a and μ_c components are given by Eqs. (2) and (3):

$$\mu_a(O_3\text{–}H_2O) = \mu(O_3)\langle\cos\theta_1\rangle + \mu(H_2O)\langle\cos\theta_2\rangle \tag{2}$$

$$\mu_c(O_3\text{–}H_2O) = \mu(O_3)\langle\sin\theta_1\rangle + \mu(H_2O)\langle\sin\theta_2\rangle. \tag{3}$$

The signs of the terms in Eqs. (2) and (3) are determined by assuming that the positive end of the H_2O dipole is oriented toward the hydrogens, while the positive end of the O_3 dipole is oriented toward the central oxygen of ozone. If induced moment contributions are neglected, then θ_2 can be obtained for a fixed value of θ_1. For the angle $\theta_1 = 121.4°$ (average of the values for the A structure) the best agreement is found for $\theta_2 = 38°$ which gives calculated values $\mu_a(O_3\text{–}H_2O) = 1.18$ D (compared to the measured value of 1.014 D) and $\mu_c = 0.69$ D (compared to the measured value of 0.552 D). The discrepancies of about 0.15 D most likely are due to the neglect of induced moments. The induced dipole effects can be estimated by assuming that water causes a larger induced moment on ozone due to the much larger dipole moment of water and assuming the magnitude of the induced moment to be 0.2 D, which is the difference between μ_T observed and the calculated difference in monomer moments. When employing Eqs. (2) and (3) with $\mu(O_3) = 0.73$ D and $\theta_1 = 121.4°$, a value $\theta_2 = 39.5°$ results for O_3–H_2O with differences between the calculated and observed μ_a and μ_c values of 0.03 D. By carrying out the calculation with the same assumptions for the moments of O_3–HDO and O_3–D_2O, we obtain values of θ_2 of 42.5° for O_3–HDO and 43.5° for O_3–D_2O with discrepancies of about 0.03 D between calculated and observed moments. These values for θ_2 show a much smaller range, 4°, than found in the structure fits in Table III where the range of the θ_2 values is 46°.

Deuterium hyperfine structure. The deuterium quadrupole coupling constants allow a further independent determination of the water orientation in the complex. If it is assumed that the electric field gradient at the deuterium nucleus does not change upon complexation, then the coupling constants of O_3–H_2O can be related to projections of the free HDO coupling constants on the inertial axes of the complex. Since the quadrupole coupling tensor of HDO is approximately symmetric about the O–D bond (*21*), the angle, α, between the O–D bond and the a-axis of the complex is given by Eq. (4).

$$eQq_{aa} \approx eQq_{O\text{–}D}[(3\langle\cos^2\alpha\rangle - 1)/2]. \tag{4}$$

Analogous expressions can be used to obtain the projection angle β along the b-axis and angle γ along the c-axis. Solutions of these expressions using the measured eQq values for O_3–HDO in Table IV and $eQq_{O\text{–}D} = 313.2$ kHz reported by Fry and Kukolich for HDO (*21*) give $\alpha = 63°$, $\beta = 58.4°$, and $\gamma = 44°$. The α and γ angles are directly related to θ_2 and yield $\theta_2 = 65°$ and $\theta_2 = 82°$, respectively. These results also indicate the influence of zero point vibrational motion since the sum of $\alpha + \gamma = 107°$ rather than 90° which is expected for a rigid molecule. Further, the angle β should be 90° if the O–D bond were rigidly located in the a, c plane as dictated by the zero μ_b dipole

component. A μ_b component of about 0.5 D would result if the equilibrium structure was represented by the angle $\beta = 58.4°$, which can be ruled out by the Stark effect analysis. As a result, the deuterium hyperfine structure does not provide a definitive answer to the value of θ_2.

Summary. To summarize the structural results, we find that structure **A** in Fig. 3 is most consistent with the spectroscopic data. The center of mass distance, R_{cm}, is 2.957(2) Å and $\theta_1 = 121.4 \pm 4°$. The value of θ_2 is poorly determined, but likely lies in the range $40° < \theta_2 < 82°$ to be consistent with the moment of inertia, dipole moment, and deuterium hyperfine structure data. In order to support these conclusions, we have appealed to theory as described in the next section. The source of the structural analysis inconsistencies may be due to the presence of a large amplitude tunneling motion which is evident in the spectrum and discussed in Section VII.

VI. THEORETICAL ANALYSIS

Ab initio calculations on the O_3–H_2O complex have been carried out at various levels of theory including Hartree–Fock (HF) and Moller–Plesset perturbation theory at second (MP2) and fourth order [MP4(SDTQ)] (*22, 23*). Test calculations on other ozone complexes (*24*) reveal that a correct description of the O_3–H_2O complex can only be expected at the MP4 level of theory. Furthermore, it is well known that an accurate description of van der Waals complexes requires a large basis set of at least $TZ + 2P$ quality. However, full MP4 geometry optimizations with more than 80 basis functions are not feasible at the moment and, therefore, we compromised by using a smaller basis set of valence $DZ + P$ quality, namely Pople's 6-31G(d, p) basis set (*25*). In this way MP4(SDTQ) geometry optimizations became feasible. Even though high accuracy of the calculations cannot be expected at this level of theory, the MP4/6-31G(d, p) approach leads to useful results when closely related forms such as **A** and **B** (Fig. 3) have to be compared. Also, it can provide a reasonable description of the electronic structure of the complex, thereby providing a basis for the discussion of its stability.

All calculations have been carried out within the symmetry constraints suggested by the experimental results. For the geometry optimization the parameters r, α_1, and α_2 defined in Fig. 4 have been used rather than parameters R_{cm}, θ_1, and θ_2 defined in Fig. 3.

In Table VII results of the MP2 and MP4 calculations are summarized. Geometry optimization of structure **A** at the MP2/6-31G(d, p) level of theory leads to an energy minimum while geometry optimization of structure **B** does not. This is not surprising since structure **B** suffers from an unfavorable electrostatic repulsion between a partially positively charged H atom and the partially positively charged central O atom of ozone. This repulsion is probably not compensated by dipole–dipole attraction between the monomer dipole moments aligned antiparallel to one another.

Reoptimization of structure **A** at the MP4(SDTQ)/6-31G(d, p) level of theory using analytic gradients (*26, 27*) leads to $R_{cm} = 2.757$ Å, $\theta_1 = 118.3°$, and $\theta_2 = 63.0°$ which in view of the limited size of the basis set used can be considered as being close to the experimental geometry of **A** ($R_{cm} = 2.957$ Å, $\theta_1 = 121.4°$, and $\theta_2 = 40°$–$82°$). Since the ozone dipole moment is underestimated both at the MP2 and the MP4/6-

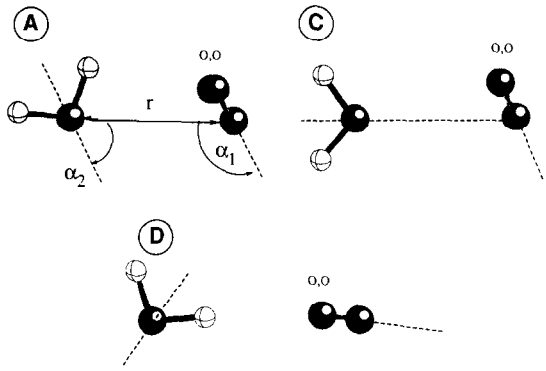

FIG. 4. Structures **A**, **C**, and **D** of the O_3–H_2O complex obtained by optimizing the geometrical parameters r, α_1, and α_2 of a number of microwave derived structures at the MP2/6-31G(d, p) level of theory. r is the distance between the central oxygen of ozone and the oxygen of water, α_1 is the angle between r and the C_2 axis of ozone, and α_2 is the angle between r and the C_2 axis of water.

31G(d, p) level (see Table VIII), electrostatic interactions between ozone and water are also underestimated leading to a R_{cm} value too short by 0.2 Å. In this connection one has to note that the calculated MP geometries of the ozone monomer (Table VIII) already bear a relatively large error compared to the experimental geometry (*28*). This has also been found by other authors (*29*).

On the other hand, there is good agreement for θ_1 (118.3° from theory versus 121.4° from the moments of inertia fits) where both theory and experiment find the terminal oxygens of ozone tilted toward the water subunit (see structure **A** in Figs. 3 and 4). The calculated orientation of the water molecule suggests that θ_2 should be close to 60° which is in agreement with the analysis of the experimental moments of inertia (see θ_2 value in first column of Table VI) and the deuterium quadrupole projection angle (θ_2 = 65°).

When scanning the potential surface of the ozone–water complex for structure **B**, two other low energy forms **C** and **D** (see Table VII and Fig. 4) have been found. In **C** one of the OH bond dipole moments is antiparallel to the ozone dipole moment, thus leading to stabilizing electrostatic interactions, even though these should be smaller than in form **A**. In form **D** one of the H atoms is oriented toward the terminal O atoms of ozone, thereby establishing some weak H bonding (the O . . . H distance is 2.40 Å, which is equal to the sum of the van der Waals radii). Forms **C** and **D** are 0.6 and 0.3 kcal/mole, respectively, higher in energy than **A** (see Table VII).

The MP4 dissociation energy of the ozone–water complex is relatively large (2.4 kcal/mole, Table VII), but it has to be corrected for basis set superposition errors (BSSE) (*30*). The BSSE corrected MP4(SDTQ)/6-31G(d, p) value for the complex stability with regard to the dissociated molecules ozone and water (Table VIII) is 0.7 kcal/mole.

The electronic structure of the O_3–H_2O complex can be described by an analysis of its electron density distribution $\rho(\mathbf{r})$. Particularly useful is an analysis of the difference electron density distribution $\Delta\rho(\mathbf{r})$ (*31*). The distribution $\Delta\rho(\mathbf{r})$ has been calculated

TABLE VII

Structural Parameters and Energies of Ozone–Water Complex Calculated at the MP2 and MP4 Level of Theory[a]

Parameter	MP2/6-31G(d,p)			MP4(SDTQ)/
Energy				6-31G(d,p)
	A	C	D	A
r	2.942	2.903	3.777	2.965
α_1	126.0	112.8	178.8	125.0
α_2	54.2	2.4	132.4	56.3
r(OO)	1.299	1.299	1.299	1.299[b]
<OOO	116.1	116.3	116.1	116.1[b]
$r(OH_1)$	0.962	0.961	0.962	0.962[b]
$r(OH_2)$	0.961	0.961	0.961	0.961[b]
<HOH	104.6	104.1	104.0	104.6[b]
ΔE[c]	0	0.62	0.29	0
$\Delta E(O_3+H_2O)$[d]	-3.55	-2.93	-3.25	-2.40
ΔE(BSSE)[e]	-1.01	-0.38	-0.71	-0.70

[a]Distances r in Å, angles α in deg, relative energies ΔE in kcal/mol for structures **A**, **C** and **D** shown in Fig. 4.

[b]Parameters from MP2/6-31G(d,p) calculation.

[c]The MP2/6-31G(d,p) energy of **A** is -301.10485 hartree, the MP4(SDTQ)6-31G(d,p) energy -301.12555 hartree.

[d]Energy relative to that of the separated molecules. See Table VIII.

[e]Energy relative to that of the separated molecules after correcting for basis set superposition errors (BSSE).

TABLE VIII

Structural Parameters and Energies of O_3 and H_2O Calculated at the MP2/6-31G(d, p) and the MP4(SDTQ)/6-31G(d, p) Level of Theory[a]

Parameter	MP2/ 6-31G(d,p)	MP4(SDTQ)/ 6-31G(d,p)	exp.[b] r_e
r(OO)	1.299	1.306	1.272
<OOO	116.3	117.2	116.8
r(OH)	0.961	0.964	0.965
<HOH	104.1	104.3	104.8
$\mu(O_3)$	0.40	0.44	0.53
$E(O_3)$	-224.87675	-224.89576	
$E(H_2O)$	-76.22245	-76.23357	

[a]Distances r in Å, angles in deg, energies E in hartree, dipole moment μ in Debye.

[b]From ref. 28 and 20.

by subtracting from the electron density distribution $\rho(\mathbf{r})$ of the O_3–H_2O complex the electron density distribution $\rho(\mathbf{r})'$ of the "procomplex." The procomplex possesses the geometry of the complex, but there are no interactions between the molecules forming the complex (*31*). The analysis of $\Delta\rho(\mathbf{r}) = \rho(\mathbf{r}) - \rho(\mathbf{r})'$ reveals at which positions in the complex negative charge is accumulated (deleted) relative to the non-interacting molecules in the procomplex. In Fig. 5 $\Delta\rho(\mathbf{r})$ is shown in the form of a contour line diagram calculated for the symmetry plane of the complex that contains H_2O and the central O atom of O_3. Solid contour lines denote $\Delta\rho(\mathbf{r}) > 0$, while dashed contour lines denote $\Delta\rho(\mathbf{r}) < 0$.

A dominating feature of $\Delta\rho(\mathbf{r})$ is the depletion of negative charge in the region between the two molecules of the complex. Any withdrawal of electron density from this region leads to a decrease of destabilizing repulsion between the electrons of H_2O and O_3. In the complex the H atoms, in particular the H atom next to the ozone molecule, H_1, lose negative charge while at the same time there is an increase of negative charge in the lone pair region of the O atom of H_2O and the terminal O atoms of O_3. In this way electrostatic attraction between H_1 and the terminal O atoms of ozone (distance: 2.5 Å) is increased. In addition, the dipole moments of H_2O (1.85 D) and ozone (0.53 D) increase upon complex formation (*24*).

We conclude that the stability of O_3–H_2O is primarily due to electrostatic attraction between the molecules forming the complex. The C_s form appears to be a result of coulomb attraction between a positively charged H_1 atom and two negatively charged terminal O atoms of O_3 since this attraction is a maximum if both O atoms are located at the same distance from H_1. Beside coulomb attraction between partially charged atoms, dipole–dipole attraction between O_3 and H_2O is the major contributing factor

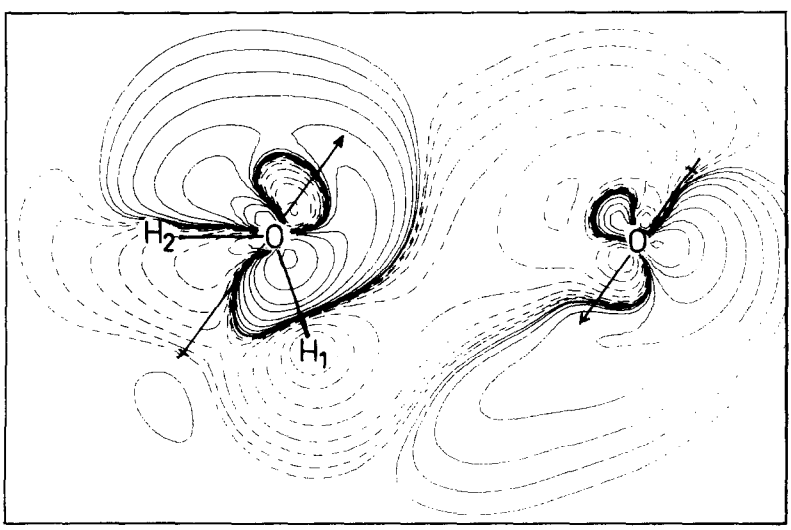

FIG. 5. Contour line diagram of the difference electron density distribution $\Delta\rho(\mathbf{r})$ calculated for the symmetry plane of the O_3–H_2O complex at the HF/6-31G(d, p) level of theory. The direction of the dipole moment vectors of O_3 and H_2O are indicated by the arrows. Note that the terminal O atoms of ozone are above and below the reference plane close to the negative end of the dipole moment vector of O_3.

to the stability of O_3–H_2O. Using the distance R_{cm} = 2.96 Å between the centers of mass of the two monomers in the complex and the experimental dipole moments of H_2O and O_3, an electrostatic stabilization energy of 0.5 kcal/mole is predicted.

VII. INTERNAL MOTION

The *a*-type transitions of O_3–H_2O and O_3–D_2O are split into two components, designated A_1 and A_2, due to an internal motion in the complex. Both *a*- and *c*-type transitions are observed for the A_1 state of O_3–H_2O and O_3–D_2O. The *a*- and *c*-type lines are pure rotational transitions and could be fit to within the experimental uncertainty of the frequency measurements with a standard Watson Hamiltonian (see Table I). For the A_2 state, the asymmetry splitting in the $K = 1$ $J = 2 \leftarrow 1$ *a*-type transition indicates large deviations from rigid rotor behavior, and the spectrum does not fit a Watson Hamiltonian presumably due to large Coriolis effects. Differences in intensities distinguish A_1 and A_2 state lines and the observed relative intensities of 1:3 and 2:1 for the A_1 and A_2 states of O_3–H_2O and O_3–D_2O, respectively, indicate the hydrogens (deuteriums) are exchanged by the motion. The large splittings of the A_1 and A_2 transitions are not strongly affected by deuteration in the complex (see Table II). This result is somewhat anomalous since the observed relative intensities suggest the hydrogens are involved in the motion, yet the splittings are not substantially reduced in O_3–D_2O. Finally, there is no evidence for two states in O_3–HDO, where one species is observed and the *a*- and *c*-type transitions fit well to a Watson Hamiltonian (see Tables III and IV).

A tunneling pathway can be visualized which involves a concerted motion of water and ozone making the reduced mass relatively insensitive to deuteration but still satisfying the nuclear spin weights. First, we assume the complex has an *a*, *c*-symmetry plane with the water and central oxygen of ozone being located in this plane. Four possible equivalent frameworks exist for O_3–H_2O and O_3–D_2O in which the hydrogen atoms and the terminal oxygens of ozone are exchanged by internal motions. As shown in Fig. 6, the [1] → [2] motion interchanges the two hydrogen atoms, the [1] → [3] motion does the same for the two terminal oxygens of ozone, and the [1] → [4] motion is a combination of the two motions above. It achieves the interchange of the hydrogens and oxygens through a geared internal rotation of both monomers and does not invert the μ_a or μ_c dipole moment directions. Dipole inversion would

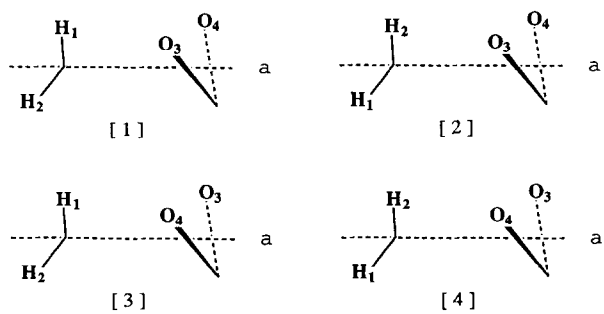

FIG. 6. Equivalent frameworks and proposed internal motion of O_3–H_2O and O_3–D_2O.

cause the transitions to be shifted up (or down) from the rigid rotor positions by the tunneling frequency separating the A_1 and A_2 levels.

By analogy to H_2O–D_2O (*10*) which has the same permutation–inversion group as do O_3–H_2O and O_3–D_2O, each asymmetric rotor level is split into four states by the motions in Fig. 6. The symmetry species of the four states are $A_1^{\pm}$, $A_2^{\pm}$, $B_1^{\pm}$, and $B_2^{\pm}$. Allowed transitions follow the selection rules $A_1^{+} \leftrightarrow A_1^{+}$, $A_2^{+} \leftrightarrow A_2^{+}$, $B_1^{+} \leftrightarrow B_1^{+}$, and $B_2^{+} \leftrightarrow B_2^{+}$. Nuclear spin weights of $g = 1, 3, 0, 0$ (O_3–H_2O) and $g = 6, 3, 0, 0$ (O_3–D_2O) result for the A_1, A_2, B_1, and B_2 states, respectively, due to exchange of spin 1/2 protons (spin 1 deuterium) and spin 0 oxygen nuclei. Since the B_1 and B_2 states have zero spin weights, the motion will give rise to two states designated A_1 and A_2.

The geared internal rotation pathway [1] → [4] is consistent with the presence of two states having spin weights of $A_1 = 1$ and $A_2 = 3$ for O_3–H_2O and $A_1 = 6$ and $A_2 = 3$ for O_3–D_2O. A coupled internal rotation of ozone and water will make the reduced mass insensitive to deuteration and explain the similar splittings in the *a*-type transitions of O_3–H_2O and O_3–D_2O. Both the *a*- and *c*-type transitions occur within the A_1 state of both O_3–H_2O and O_3–D_2O. There is no evidence for inversion transitions between these states. The large splittings and the nonrigid rotor behavior of the A_2 state suggest that the barrier to the [1] → [4] motion is low. For the O_3–HDO isotopic species, the motion does not exchange equivalent hydrogen nuclei. Hence, there is no splitting possible, and two distinct pure rotational spectra corresponding to isotopic substitution of deuterium at each of the two nonequivalent hydrogen positions are expected. Since only one isotopic species of O_3–HDO was observed, the second isotopic form must be of higher energy and is not populated in the 1-K beam.

An alternative motion which is qualitatively consistent with the spectroscopic data involves nearly free internal rotation of water. Recent work with Ar–H_2O finds the H_2O unit is undergoing slightly hindered internal rotation in a weakly anisotropic potential (*32, 33*). Like ozone–water the splitting in the two observed internal rotor states of Ar–H_2O is not reduced by deuteration in Ar–D_2O (*33*). Complete assignments of the A_2 states of O_3–H_2O and O_3–D_2O and the development of a Hamiltonian are needed to understand the internal motion which gives rise to the two states in O_3–H_2O and O_3–D_2O.

VIII. DISCUSSION

Some interesting structural and dynamical comparisons can be made between the Ar–O_3, Ar–SO_2 complexes and the O_3–H_2O, SO_2–H_2O complexes. In both Ar–O_3 and Ar–SO_2, the argon atom is located above the molecular plane along a line which is approximately perpendicular to this plane and connects the center of mass of the molecule (O_3 or SO_2) to argon (*1, 5, 34*). The separation between argon and the triatomic center of mass is approximately equal to the sum of the two van der Waals radii for argon and oxygen, as well as argon and sulfur.

O_3–H_2O and SO_2–H_2O have *a*, *c*-symmetry planes which bisect the OSO and OOO angles and contain the water and unique oxygen in O_3–H_2O and the water oxygen and sulfur in SO_2–H_2O (*35*). However, ozone is tilted in the opposite sense with respect to R_{cm} than is SO_2 since $\theta_1 = 121.5°$ for O_3–H_2O and $\theta_1 = 69.7°$ for SO_2–H_2O. The hydrogens are located in the *a*, *c* plane for O_3–H_2O, while in the SO_2–H_2O

complex the hydrogens lie at 90° to the a, c plane. For SO_2–H_2O the structure is not hydrogen-bonded. In O_3–H_2O it is not clear whether the hydrogen adjacent to the terminal oxygens of ozone can be considered a weak hydrogen-bond due to the uncertainty in θ_2 which gives a range of 2.7 to 3.1 Å for this H . . . O distance.

The center of mass distances are almost identical with R_{cm} = 2.957 Å for O_3–H_2O and R_{cm} = 2.962 Å for SO_2–H_2O. Since the water oxygen to terminal ozone oxygen distance is 3.007 Å, the classical van der Waals oxygen radius of 1.5 Å is consistent with the observed value in O_3–H_2O. The opposite tilt of SO_2 (in SO_2–H_2O) compared to O_3 (in O_3–H_2O) places the sulfur rather than the oxygens of SO_2 closest to the water oxygen. This S. . .O distance is 2.824 Å which is short compared with the sum of the classical sulfur (1.85 Å) and oxygen (1.5 Å) van der Waals radii. If the value of 1.5 Å for the oxygen van der Waals radii in O_3–H_2O is used for SO_2–H_2O, then the effective sulfur van der Waals radius is calculated to be ~1.3 Å. It was suggested that SO_2 is a better Lewis acid toward H_2O than O_3 which produces a stronger van der Waals bond in the SO_2–H_2O complex (*35*). Evidence for this explanation was presented by determining the van der Waals stretching force constant k_s and vibrational frequency ω_s from Δ_J using a pseudodiatomic model. These quantities are estimated to be larger for SO_2–H_2O (k_s = 0.053 mdyne/Å; ω_s = 80.1 cm^{-1}) than O_3–H_2O (k_s = 0.038 mdyne/Å, ω_s = 70.3 cm^{-1}) as expected if SO_2–H_2O is more strongly bound than O_3–H_2O.

The internal motions in Ar–O_3 and Ar–SO_2 are quite different from O_3–H_2O and SO_2–H_2O. Both of the argon complexes undergo high-frequency inversions (460 MHz for Ar–O_3 and 975 MHz for Ar–SO_2) (*1, 34*). The motion inverts the dipole moment along the c principal axis which gives rise to μ_c-type rotation–inversion transitions. Attempts to describe the van der Waals potentials from force fields derived from the centrifugal distortion constants show that the potential for Ar–SO_2 is very anisotropic with strong coupling of the van der Waals vibrations (*1*). Unlike Ar–SO_2, Ar–O_3 is well described by the semirigid model giving reasonable force constants and frequencies for the van der Waals vibrations.

For both O_3–H_2O and SO_2–H_2O, the tunneling motion likely involves internal rotation of the monomer subunits because there is no evidence for inversion splittings in the a- and c-type transitions. The observed splittings of the two states are a factor of 10 or more greater in O_3–H_2O than reported for SO_2–H_2O. This suggests that the barrier to the tunneling motion is substantially larger in SO_2–H_2O. The higher barrier in SO_2–H_2O also is in agreement with the ability to fit the A_1 and A_2 states to a Watson Hamiltonian for SO_2–H_2O, but only the A_1 state for O_3–H_2O is well behaved. Complete deuteration of water in the SO_2–H_2O complex substantially reduces the tunneling splitting attributed to an internal rotation dominated by water in the complex. For the ozone–water complex, the splittings of the a-type J = 2–1 transitions are roughly the same in O_3–H_2O and O_3–D_2O. Unlike SO_2–H_2O, this suggests that the motion may involve a concerted motion of ozone and water such as the geared internal rotation shown in Fig. 6 or nearly free internal rotation of water as recently observed in Ar–H_2O (*32, 33*). More complete spectral assignments for the A_2 state of O_3–H_2O and O_3–D_2O are needed, and a model must be developed to fit the A_2 state transitions in order to understand the unusual internal motion in ozone–water.

The gas phase results presented here can be compared to a recent infrared matrix

isolation study of O_3–H_2O (*36*). From the infrared absorption fundamentals of complexed water and force field calculations, it was found that the two OH oscillators are nonequivalent which is consistent with our structural analysis. The results indicate that the complex is very weakly hydrogen bonded even when compared to unsaturated hydrocarbon complexes (*37*). Since one hydrogen of water is found within the range of 2.7 to 3.1 Å of the two terminal oxygens of ozone, a weak bridging hydrogen bond is also possible in the gas phase complex. Furthermore, the stabilization energy of 0.7 kcal/mole from the ab initio calculation reported here also indicates that the complex is weakly bound. With a large excess of ozone, new infrared absorption bands of complexed water in the matrix were assigned to $(O_3)_2$–H_2O. In our gas phase study the ozone concentrations were not high, and no strong unassigned lines were observed which required both ozone and water.

ACKNOWLEDGMENTS

The authors are grateful to Dr. L. H. Coudert for helpful discussions related to the symmetry designations of the tunneling states and the nuclear spin statistical weights of these states. They also thank Drs. G. T. Fraser and J. T. Hougen for critically reading the manuscript. DC thanks the NSC, Linköping, Sweden for support through computer time. Calculations have been supported by the NFR, Sweden. This research was partially supported by a grant from Research Corporation (CWG).

RECEIVED: December 4, 1990

REFERENCES

1. J. S. MUENTER, R. L. DELEON, AND A. YOKOZEKI, *Faraday Discuss. Chem. Soc.* **73,** 63–70 (1982).
2. T. R. Dyke, *Top. Curr. Chem.* **120,** 85–113 (1984).
3. A. C. LEGON AND D. J. MILLEN, *Chem. Rev.* **86,** 635 (1986).
4. S. E. NOVICK, *in* "Structure and Dynamics of Weakly Bound Molecular Complexes" (A. Weber, Ed.), p. 201, Reidel, Dordrecht, 1987.
5. R. L. DELEON, K. M. MACK, AND J. S. MUENTER, *J. Chem. Phys.* **71,** 4487–4491 (1979).
6. J. Z. GILLIES, C. W. GILLIES, R. D. SUENRAM, F. J. LOVAS, AND W. STAHL, *J. Am. Chem. Soc.* **111,** 3073–3084 (1989).
7. J. G. CALVERT, A. LAZRUS, G. L. KOK, B. G. HEIKES, J. G. WALEGA, J. LIND, and C. A. CANTRELL, *Nature* **317,** 27–35 (1985).
8. T. J. BALLE AND W. H. FLYGARE, *Rev. Sci. Instrum.* **52,** 33–45 (1981); F. J. LOVAS AND R. D. SUENRAM, *J. Chem. Phys.* **87,** 2010–2020 (1987).
9. F. J. LOVAS, R. D. SUENRAM, G. T. FRASER, C. W. GILLIES, AND J. ZOZOM, *J. Chem. Phys.* **88,** 722–729 (1988).
10. L. H. COUDERT, F. J. LOVAS, R. D. SUENRAM, AND J. T. HOUGEN, *J. Chem. Phys.* **87,** 6290–6299 (1987).
11. T. R. DYKE, K. M. MACK, AND J. S. MUENTER, *J. Chem. Phys.* **66,** 498–510 (1977).
12. H. M. PICKETT, E. A. COHEN, AND J. S. MARGOLIS, *J. Mol. Spectrosc.* **110,** 186–214 (1985).
13. J. A. ODUTOLA AND T. R. DYKE, *J. Chem. Phys.* **72,** 5062–5070 (1980).
14. J. K. G. WATSON, *in* "Vibrational Spectra and Structure" (J. R. Durig, Ed.), Vol. 6, p. 1, Elsevier, Amsterdam, 1977.
15. E. J. CAMPBELL, W. G. READ, AND J. A. SHEA, *Chem. Phys. Lett.* **94,** 69–72 (1983).
16. J. M. L. J. REINHARTZ AND A. DYMANUS, *Chem. Phys. Lett.* **24,** 346–351 (1974); J. S. MUENTER, *J. Chem. Phys.* **48,** 4544–4547 (1968).
17. S. GOLDEN AND E. B. WILSON, *J. Chem. Phys.* **16,** 669–685 (1948).
18. W. GORDY AND R. L. COOK, "Microwave Molecular Spectra," Wiley, New York, 1970.
19. F. J. LOVAS, *J. Phys. Chem. Ref. Data* **7,** 1445–1750 (1978).
20. R. L. COOK, F. C. DELUCIA, AND P. HELMINGER, *J. Mol. Spectrosc.* **53,** 62–76 (1974).

21. H. A. FRY AND S. G. KUKOLICH, *J. Chem. Phys.* **76,** 4387–4391 (1982).
22. J. A. POPLE, J. S. BINKLEY, AND R. SEEGER, *Int. J. Quant. Chem. Symp.* **10,** 1–19 (1976).
23. R. KRISHNAN AND J. A. POPLE, *Int. J. Quant. Chem.* **14,** 91–100 (1978); R. KRISHNAN, M. J. FRISCH, AND J. A. POPLE, *J. Chem. Phys.* **72,** 4244–4245 (1980).
24. D. CREMER, to be published.
25. P. C. HARIHARAN AND J. A. POPLE, *Chem. Phys. Lett.* **16,** 217–219 (1972).
26. J. GAUSS AND D. CREMER, *Chem. Phys. Lett.* **138,** 131–136 (1987).
27. J. GAUSS AND D. CREMER, *Chem. Phys. Lett.* **153,** 303–308 (1989).
28. T. TANAKA AND Y. MORINO, *J. Mol. Spectrosc.* **33,** 538–551 (1970).
29. J. F. STANTON, W. N. LIPSCOMB, D. H. MAHERS, AND R. J. BARTLETT, *J. Chem. Phys.* **90,** 1077–1082 (1989).
30. S. F. BOYS AND F. BERNARDI, *Mol. Phys.* **19,** 553–566 (1970).
31. D. CREMER AND E. KRAKA, *J. Phys. Chem.* **90,** 33–40 (1986).
32. R. C. COHEN, K. L. BUSAROW, K. B. LAUGHLIN, G. A. BLAKE, M. HAVENITH, Y. T. LEE, AND R. J. SAYKALLY, *J. Chem. Phys.* **89,** 4494–4504 (1988); R. C. COHEN, K. L. BUSAROW, Y. T. LEE, AND R. J. SAYKALLY, *J. Chem. Phys.* **92,** 169–177 (1990); J. M. HUTSON, *J. Chem. Phys.* **92,** 157–168 (1990).
33. G. T. FRASER, F. J. LOVAS, R. D. SUENRAM, AND K. MATSUMURA, *J. Mol. Spectrosc.*, in press (1990).
34. R. L. DELEON, A. YOKOZEKI, AND J. S. MUENTER, *J. Chem. Phys.* **73,** 2044–2048 (1980).
35. K. MATSUMURA, F. J. LOVAS, AND R. D. SUENRAM, *J. Chem. Phys.* **91,** 5887–5894 (1989).
36. L. SCHRIVER, C. BARREAU, AND A. SCHRIVER, *Chem. Phys.* **140,** 429–438 (1990).
37. A. ENGDAHL AND B. NELANDER, *Chem. Phys. Lett.* **113,** 49–55 (1985).